Avalanches, precursors, and finite-size fluctuations in a mesoscopic model of amorphous plasticity

Mehdi Talamali,[1] Viljo Petäjä,[2] Damien Vandembroucq,[1] and Stéphane Roux[3]
[1]*Laboratoire PMMH, UMR 7636 CNRS/ESPCI/Univ. Paris 6 UPMC/Univ. Paris 7 Diderot, 10 rue Vauquelin, F-75231 Paris cedex 05, France*
[2]*Laboratoire SVI, UMR 125 CNRS/Saint-Gobain, 39 quai Lucien Lefranc, F-93303 Aubervilliers cedex 05, France*
[3]*LMT-Cachan, ENS de Cachan/CNRS-UMR 8535/Univ. Paris 6 UPMC/PRES UniverSud Paris, 61 Avenue du Président Wilson, F-94235 Cachan cedex, France*
(Received 24 March 2011; published 29 July 2011)

We discuss avalanche and finite-size fluctuations in a mesoscopic model to describe the shear plasticity of amorphous materials. Plastic deformation is assumed to occur through series of local reorganizations. Yield stress criteria are random while each plastic slip event induces a quadrupolar long-range elastic stress redistribution. The model is discretized on a regular square lattice. Shear plasticity can be studied in this context as a depinning dynamic phase transition. We show evidence for a scale-free distribution of avalanches $P(s) \propto S^{-\kappa}$ with a nontrivial exponent $\kappa \approx 1.25$ significantly different from the mean field result $\kappa = 1.5$. Finite-size effects allow for a characterization of the scaling invariance of the yield stress fluctuations observed in small samples. We finally identify a population of precursors of plastic activity and characterize its spatial distribution.

DOI: 10.1103/PhysRevE.84.016115 PACS number(s): 62.20.F−, 83.80.Ab, 45.70.Ht

I. INTRODUCTION

While traditionally described in continuum mechanics by constitutive laws at macroscopic scale, it has progressively appeared in the last two decades that the mechanical behavior of materials was not as smooth and regular as anticipated. In particular crack propagation in brittle materials and plastic flow in crystalline solids have been shown to exhibit jerky motion and scale-free spatiotemporal correlations [1–3].

Beyond its obvious fundamental interest, the understanding of intermittence and intrinsic fluctuations in mechanics of materials and their consequences at macroscopic scale is of direct importance for engineering applications: Among other examples a quantitative assessment of risk of failure would allow us to better determine security margins that stay rather uncontrolled (and often overestimated); and a theoretical understanding of finite-size effects would allow us to model the mechanical behavior of small pieces, a question of crucial interest with the rapid technological development of MEMS and NEMS (Micro- or Nano- Electro-Mechanical Systems).

Concepts such as avalanches and criticality have thus been increasingly used in that context to describe and model fracture and plasticity. In particular, the paradigm of the depinning transition has been shown to be extremely appealing to model such nonlinear phenomena at mesoscopic scale [4–10]. Such a formalism indeed naturally captures the competition between the disorder of local thresholds (toughness for crack propagation, yield stress for plastic deformation) and elastic interactions that couple local mechanical events (crystallographic slip, crack advance). A critical threshold naturally emerges at macroscopic scale that separates a static phase (crack propagation or plastic deformation stops after a finite excursion) from a mobile phase (free propagation or deformation). As usual, this dynamic phase transition can be characterized by a set of critical exponents.

While crystalline plasticity or crack propagation rely on rather solid grounds (theory of dislocation and linear elastic fracture mechanics, respectively), the understanding of plastic deformation in amorphous materials such as oxide or metallic glasses is still in its infancy. In the absence of crystalline lattice, plasticity seems to originates from a series of very local structural rearrangements [11,12]. Beyond this first level of description, any local reorganization has to be accommodated by the surrounding elastic matrix and induces internal stress [13–15]. These local plastic events thus do not occur independently but in a strong correlated way.

We recently introduced a mesoscopic model of plasticity in amorphous materials [16]. Following an earlier work [9] we developed a scalar discrete model on a regular lattice with a random yield stress. The local slip occurring when the shear stress satisfies the plastic criterion is accompanied by an elastic stress redistribution of quadrupolar symmetry [17,18], which corresponds to the elastic response of the surrounding matrix to this Eshelby-like plastic inclusion [19]. Although originally due to the quadrupolar symmetry of the elastic interaction, one recognizes in this short description the two ingredients of a depinning model: a random threshold field and an elastic interaction.

In a previous paper [16] we focused on the competition between localization and diffusion that naturally emerges from the peculiar symmetry of the elastic interaction. Some directions being favored, plastic deformation forms shear bands that span the entire lattice. This localization is, however, not persistent, and after they grow to the size of the system, shear bands tend to diffuse throughout the lattice. In particular we could find evidence for anisotropic strain correlations that are strikingly similar to those recently observed in an atomistic study of a binary Lennard-Jones glass under compression [20,21].

In the present paper, a particular focus is given to the critical properties of the model. We recall in Sec. II the definition of the model and its salient properties. Avalanches are quantitatively characterized in Sec. III. Finite-size fluctuations close to the

critical point are analyzed in Sec. IV. Characterization of avalanche precursor sites is discussed in Sec. V. Section VI concludes this paper.

II. BRIEF DESCRIPTION OF THE MODEL

A detailed description of the model can be found in Ref. [16]. Let us simply summarize here the main points.

We consider an elastically homogeneous material in plane deformation geometry under shear. Discretization is performed on a square lattice with biperiodic boundary conditions at a scale that is larger than the size of a typical rearrangement. This scale is to be large enough to allow the use of continuum elasticity and to neglect elastic inhomogeneities. At a large scale, we impose a pure shear load $\sigma_{xx} = -\sigma_{yy}$ and $\sigma_{xy} = 0$.

A simplification consists of assuming that local rearrangements induce an elementary plastic shear with the same symmetry as the macroscopic imposed macroscopic shear. We thus consider neither volumetric change nor orientation disorder for the shear principal axis at the microscopic scale. Consequently, although the model is based on a genuine two-dimensional (2D) elastic description, the tensorial nature of the stress $\boldsymbol{\sigma}$ and strains $\boldsymbol{\varepsilon}$ plays no role. Scalar (equivalent) stress $\sigma \equiv \sigma_{xx} - \sigma_{yy}$ and strain $\varepsilon \equiv \varepsilon_{xx} - \varepsilon_{yy}$ can be defined. The latter scalar stress (resp. strain) component will be called "stress" (resp. "strain") for simplicity in the following. The criterion for yielding characterizes the local configuration of atoms, and hence will display some variability. A local yield threshold for each discrete site $\boldsymbol{x}$ as $\sigma_\gamma(\boldsymbol{x})$ is introduced; this quantity will be treated as a random variable in what follows. For all sites, the same statistical distribution will be used, chosen for simplicity as a uniform distribution over the interval $[0; 1]$. The specific form of this distribution plays no role in the scaling features addressed below.

The stress σ is a sum of the externally applied stress Σ_{ext} and the residual stress σ_{res} induced by the previous rearrangements of other regions of the system. Thus, the local scalar yield criterion for site $\boldsymbol{x}$ can be rewritten as

$$\Sigma_{\text{ext}} + \sigma_{\text{res}}(\boldsymbol{x}) = \sigma_\gamma(\boldsymbol{x}), \tag{1}$$

where σ_γ is the local yield stress. Here and in the following we use upper (lower) case symbols for macroscopic (microscopic) quantities.

Once this criterion is satisfied at site $\boldsymbol{x}$, the material experiences there an incremental slip η increasing the local plastic strain: $\varepsilon_p(\boldsymbol{x}) \to \varepsilon_p(\boldsymbol{x}) + \eta$. Similarly to the yield thresholds, the slip value η is drawn randomly from the uniform distribution, $[0; d]$ if not otherwise stated. As shown in Fig. 1(a) this local slip induces in turn a quadrupolar elastic stress redistribution [16–18] $\sigma_{\text{res}}(r,\theta) \to \sigma_{\text{res}}(r,\theta) + \eta\cos(4\theta)/r^2$.

In order to account for the local structural change that occurred, the local yield stress is renewed by drawing a new (uncorrelated) random value for $\sigma_\gamma(\boldsymbol{x})$. It is assumed that there is no persistence in the local yield stress.

Quasistatic driving conditions are considered, using *extremal dynamics*; i.e., the imposed external loading Σ_{ext} is tuned at each time step, t at the current yield stress value, Σ_c, such that only one site can slip at a time:

$$\begin{aligned}\Sigma_{\text{ext}}(t) &= \Sigma_c \\ &= \min_{\boldsymbol{x}}[\sigma_\gamma(\boldsymbol{x}) - \sigma_{\text{res}}(\boldsymbol{x})] \\ &= \sigma_\gamma(\boldsymbol{x}^*(t)) - \sigma_{\text{res}}(\boldsymbol{x}^*(t)),\end{aligned} \tag{2}$$

where $\boldsymbol{x}^*(t)$ is the extremal site at time t. Note, however, that "time," t, is used here as a simple way of counting and ordering events. On average, time is simply proportional to the total

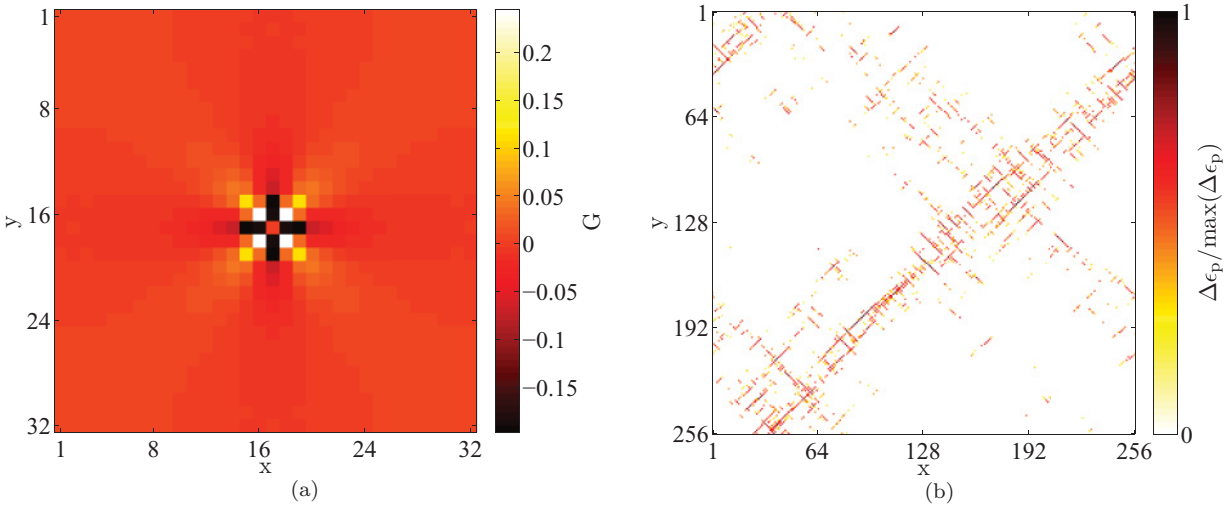

FIG. 1. (Color online) (a) Map of the quadrupolar elastic interaction G used in the model. The discretization is performed in Fourier space, and a inverse Fourier transform gives in the direct space the Green function satisfying the biperiodic boundary conditions of the problem. (b) Map of cumulated plastic activity obtained for an averaged cumulated plastic strain $\Delta\varepsilon_p = 0.01$ taken at $\varepsilon_p = 1.0$ (strain is expressed in arbitrary (infinitesimal) units). A clear localization of the plastic deformation is observed. Note that this localization behavior is nonpersistent (see Ref. [16] for details on the competition between localization and diffusion of the plastic deformation).

plastic strain imposed on the system, $\langle \epsilon_p \rangle = tdL^{-2}/2$. The plastic strain field is thus simply

$$\epsilon_p(\boldsymbol{x},t) = \sum_1^t \eta(t)\delta(\boldsymbol{x} - \boldsymbol{x}^*(t)). \tag{3}$$

In Ref. [16] we discussed the mechanical behavior of this model, and in particular we could make evidence for anisotropic plastic strain correlations, signaling the formation of shear bands as illustrated in Fig. 1(b), which, however, were not persistent and diffused throughout the system over long times. Under application of shear, a transient hardening stage was observed before the shear stress eventually saturates. This original phenomenon in the context of amorphous materials (in crystalline material hardening is usually associated with dislocation pinning by impurities or dislocation interactions) was interpreted as a consequence of the progressive exhaustion of the weakest sites of the system (reminiscent of self-organized critical systems). Plastic strain fluctuations were shown to exhibit a nontrivial scaling: Its standard deviation $\rho(\varepsilon_p)$ grows as $\rho(\varepsilon_p) \propto \varepsilon_p^{\alpha}$ with $\alpha \approx 0.75$ in the transient regime, and, in the stationary regime, the power spectrum of plastic strain was shown to exhibit an anisotropic scaling $S(q,\theta) \propto a(\theta)q^{-\alpha(\theta)}$ with $\alpha(\theta)$ obeying a quadrupolar-like symmetry. In particular, in the direction of the shear bands, we obtained $\alpha_{\pi/4} \approx 1.7$.

III. AVALANCHE BEHAVIOR

As discussed above, while intermittence and avalanches were first identified in earthquake dynamics, biological evolution [22], or magnetism [23,24], in recent years researchers have also shown their interest for the framework of mechanics of materials.

In the context of plasticity of crystalline materials, a significant amount of results have been obtained over the last decade (see, e.g., the comprehensive review by Zaiser about scale invariance in plastic flow [2]). Acoustic emission measurements performed on ice or metal monocrystals have shown a power-law distribution of the energy $P(E) \propto E^{-\kappa}$ with $\kappa \approx 1.6$ for ice [25] and $\kappa \approx 1.5$ for hcp metals and alloys [26]. The case of polycrystal is somewhat more complex since not only a grain-size-related cutoff appears in the avalanche distribution but the power-law exponent is also significantly lowered [25]. Performing nano-indentation measurements on Nickel monocrystals, Dimiduk *et al.* found evidence for a scale-free intermittent plastic flow and estimated $\kappa \approx 1.5$–1.6 [27].

Very recently analogous analysis could be performed on metallic glass samples. Sun *et al.* [28] measured the distributions of stress drops occurring in the strain stress curve for various metallic glass samples under compression. Scale-free distributions were observed with a power-law exponent $\kappa \in [1.37$–$1.49]$.

Various models have been designed that capture this avalanche behavior in plasticity at least from a qualitative point of view. Dislocation dynamics [1] and phase field [2] models have, for instance, been used in that purpose in the case of crystal plasticity. In the same context, Moretti and Zaiser [2,29] developed at mesoscopic scale a model very similar to the one presented here since it integrates some local yield randomness. A significant difference stems from their account of short-range interaction between dislocations moving on close slip planes. This local elastic interaction thus adds up and competes with the long-range interaction ensuring compatibility. This model was then used to analyze slip avalanches in crystal plasticity [30], and a scale-free behavior was obtained with a power-law exponent $\kappa = 1.5$. Special attention was given to the cutoff of the scale-free behavior, which could be associated to the finite stiffness of a testing machine and to the hardening behavior of the material. Recently Salman and Truskinovsky presented a model based on coupled Frenkel-Kontorova chains from which they could derive an integer-valued automaton [31]. In both versions of the model the dissipated energy was shown to exhibit power-law avalanches with the same exponent $\kappa = 1.6$.

In the field of amorphous plasticity, most numerical results were obtained using atomistic methods. Recently, in the framework of deformation of two-dimensional Lennard-Jones model glasses, Maloney and Robbins [20,21] obtained a linear dependence of the mean avalanche size with system size. Lemaitre, Caroli, and Chattoraj looked at the rate and termal dependence of the avalanches distribution [32,33] and showed that the athermal avalanche dynamics remain essentially unperturbed.

In a kinetic Monte Carlo study at mesoscopic scale, Homer *et al.* [34] identified different (stress- and temperature-dependent) correlation behaviors of shear transformation zones leading either to an avalanche-like behavior or to an homogeneous flow. Still at mesoscopic scale, apart from the earlier version of the present model that considered antiplane geometry, mean-field models [35] have been developed by Ben-Zion, Dahmen, and collaborators in the following of a model designed by Ben-Zion and Rice to capture earthquakes dynamics [36]. Again this class of models is very close to the one presented here with a significant difference concerning the elastic interaction, which is assumed to be mean field. These models predict a universal scale-free avalanche distribution with a power-law exponent $\kappa = 1.5$.

A. Definition and scale-free behavior

While avalanches are rather easily defined experimentally or in real-dynamics simulations, they need to be reconstructed from the fluctuating force signal in the case of depinning models driven through the extremal dynamics rules [37,38]. Following Ref. [38], avalanches are defined by introducing a small but nonzero stiffness k in the external driving as illustrated in Fig. 2(a) where the bold line of slope $-k$ represents the external driving stress. With the increasing plastic strain the external stress is decreased linearly by a quantity $k\Delta t$, where Δt is the number of iteration steps from the avalanche initiation. As soon as the driving stress drops below the current critical value σ_c, the avalanche stops. The external spring is then loaded up to σ_c and triggers a new avalanche. Far from being artificial, this procedure naturally mimics the effect of the finite stiffness of an experimental testing machine, or the elasticity of the medium surrounding the active site [30]. Based on the latter argument, the thermodynamic limit of a large-scale separation between that of the STZ, and that of the

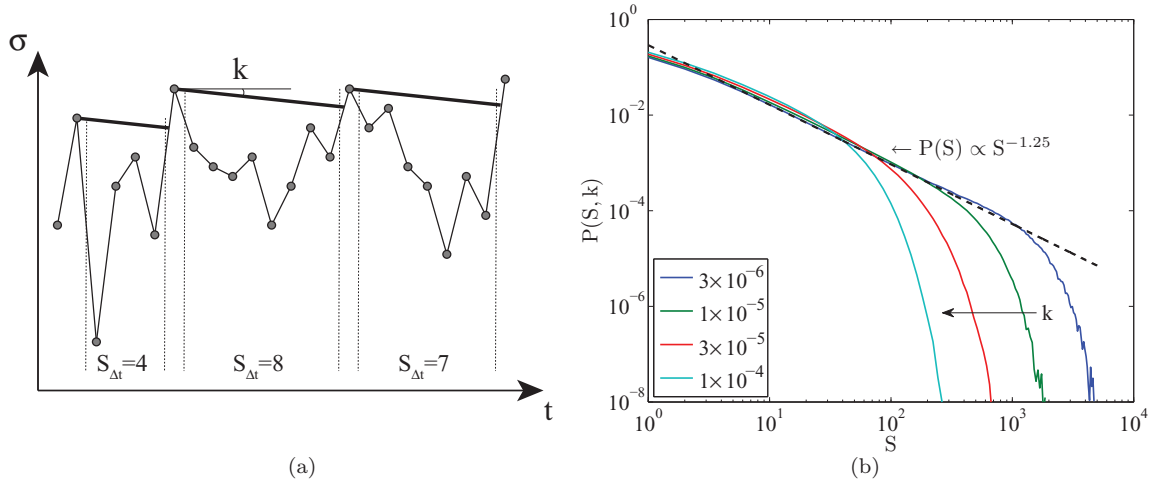

FIG. 2. (Color online) (a) Sketch of the current yield stress (as obtained in extremal dynamics) (symbol ○) and of the external stress when the system is coupled to a spring of constant k. Avalanches are defined as the intervals where the external stress remains larger than the yield stress. A new avalanche is initiated at the next maximum yield stress after arrest. (b) Distributions of avalanche sizes $P(S,k)$ for a system of size $L = 256$ and (from right to left) different values of spring constants $k = 3 \times 10^{-6}$, 10^{-5}, 3×10^{-5}, 10^{-4}. A power-law behavior $P(S,k) \propto S^{-\kappa}$ of exponent $\kappa \approx 1.25$ (dashed line) is observed with a cutoff increasing as the spring constant decreases.

medium is reproduced for a vanishing stiffness, i.e., as for an ideal stress-controlled experiment. One may also note that an ideal strain-controlled experiment would be obtained for an infinite stiffness.

The present definition size of avalanches $S = \Delta t$ should not be confused with the duration of an avalanche measured in real time. The underlying extremal dynamics gives no information about real time scales. The size S of an avalanche is, however, directly related to the strain ε_S experienced by the medium through $\varepsilon_S = S\langle\eta\rangle/L^2$ where $\langle\eta\rangle$ is the average of the random incremental local slip η.

The avalanche size distributions $P(S,k)$ corresponding to various stiffness values k are shown in Fig. 2(b). We obtain a scale-free behavior over a domain bounded by a stiffness-dependent cutoff (the lower the stiffness the larger the scaling domain). Up to the cutoff size S^* avalanche distributions follow a power law of exponent $-\kappa$ with $\kappa = 1.25 \pm 0.05$ over three decades. This excludes the mean field value $\kappa = 1.5$ as observed in mean-field models.

The present estimate $\kappa = 1.25 \pm 0.05$ is also different from the results obtained on the dislocation-based models by Zaiser *et al.* [29,30] and by Salman and Truxskinovsky [31], who observe larger values of the scaling exponent $\kappa = 1.5$–1.6. The most salient difference between these models and the present one is their account of short scale interactions between dislocations, absent in the present model. We note, however, that recent results [39,40] obtained in yet a different framework, the propagation of an interfacial crack front, recently show avalanches with the very same exponent $\kappa = 1.25$ as in the present model. This observation may be far more than a simple coincidence. Indeed, as shown above, most of the plastic events occur along the directions at $\pm\pi/4$ along which the Eshelby elastic interaction obeys the same spatial dependence in $1/r^2$ as the long-range elastic interaction characteristic of the interfacial crack growth. The latter model may then be viewed as a ultimate one-dimensional reduction of the present model of amorphous plasticity.

B. Avalanche cutoff

As discussed in Ref. [30] we thus could check that the introduction of a Gaussian cutoff allows us to obtain reasonable fits of the full set of data:

$$P(S) \sim \Delta S^{-\kappa} \exp\left[-\left(\frac{S}{S^*}\right)^2\right]. \tag{4}$$

This gives us the opportunity to test the dependence of the avalanche cutoff S^* on the "machine stiffness" k. Note here that in the framework of extremal dynamics, obtaining a size-independent mechanical behavior (stress versus strain) requires the change of variable $\varepsilon = t/L^2$ to be performed, with t being the avalanche size as above defined. Similarly, this leads to rewrite the stiffness as $k = K/L^2$, K being an elastic constant independent of the system size. Looking at Fig. 3(a), which displays the dependence of the avalanche cutoff size, this allows us to distinguish between two scaling regimes depending on whether the elastic constant K is smaller or larger than $K^* = 1$:

$$S^* \propto \begin{cases} L/K & \text{for} \quad K < K^* \\ L/\sqrt{K} & \text{for} \quad K > K^* \end{cases}. \tag{5}$$

In both cases we recover that the avalanche cutoff scales linearly with the system size L, consistent with results by Zaiser and Nikitas [30]. As illustrated in Fig. 4, a closer look at the spatial structure shows that the avalanches are highly anisotropic, and once again we recover the quadrupolar symmetry of the elastic interaction. For large values of K, avalanches remain mainly one-dimensional, while for lower values of K, two-dimensional-like patterns start to appear. One recovers here the competition between localization (at short times) and diffusion (at longer times) as discussed in Ref. [16].

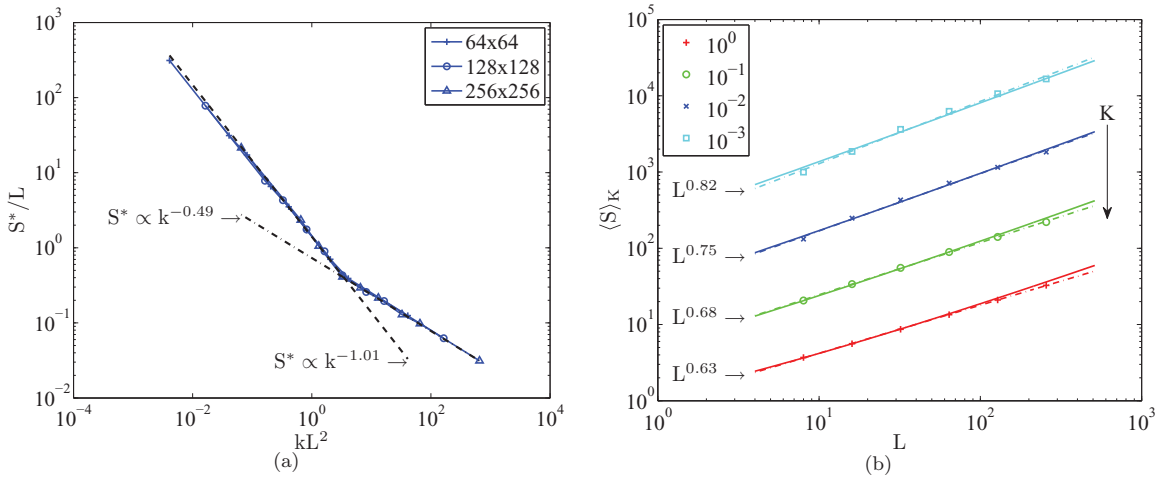

FIG. 3. (Color online) (a) Scaling of the avalanche cutoff S^* vs the rescaled stiffness $K = kL^2$. The cutoff S^* scales linearly with the system size L but exhibits either an inverse or an inverse square root dependence on the stiffness K depending on K is lower or larger than the characteristic stiffness $K^* = 1$. (b) Mean avalanche size $\langle S\rangle_K$ dependence on system size L for stiffness values $K = 10^{-3}, 10^{-2}, 10^{-1}, 1$. The simulation data are shown as symbols while the analytic expression Eq. (6) provides the continuous curves. The dash-dotted lines show the apparent scaling associated with these different cases. The apparent scaling exponents are very dependent on the stiffness value.

C. Typical size of avalanches

With this knowledge about the avalanche cutoff the typical size $\langle S\rangle$ of an avalanche can thus be estimated:

$$\langle S\rangle \approx \frac{\int_1^{S^*} s^{1-\kappa}\, ds}{\int_1^{S^*} s^{-\kappa}\, ds} \approx \frac{\kappa-1}{2-\kappa}\,\frac{(L/K^{\upsilon})^{2-\kappa}-1}{1-(L/K^{\upsilon})^{1-\kappa}}, \qquad (6)$$

where $\kappa \approx 1.25$, $\upsilon = 1$, or $\upsilon = 1/2$ depending on whether $K < K^*$ or $K > K^*$.

In Fig. 3(b), we displayed the average avalanche size $\langle S\rangle$ versus the system size L for several values of the elastic constant K. Numerical results are well reproduced by the analytical equation (6). Note that as soon as the elastic constants approaches $K^* = 1$, the apparent scaling can be very different from the naive scaling obtained at very large sizes K or low values of K: $\langle S\rangle \propto (L/E)^{\beta}$ where $\beta = 2-\kappa \approx 0.75$. The value of the machine stiffness in experimental testing is thus prone to affect the apparent scaling of the typical size of avalanches. Albeit the quality of the fits to power laws is quite satisfactory, we believe that the apparent dependence of the exponent with k is the mere reflection of the corrections, which can be rationalized by the above argument. The present results should be compared with those obtained by Maloney and Lemaître [13] who measured an an average avalanche size $\langle S_{\Delta t}\rangle \propto L$ on Lennard-Jones two-dimensional model glasses under quasistatic shear and with those of Lemaître and Caroli [41], $\langle S_{\Delta t}\rangle \propto L$ or $L^{0.3}$ for a mean-field model based on an effective mechanical noise accounting for the elastic interactions.

IV. CRITICAL THRESHOLD AND FINITE-SIZE FLUCTUATIONS

As discussed in the introduction, the rapid development of micro- and nano-electromechanical systems is a strong motivation for the understanding of their mechanical behavior. In such systems the ratio between the "micro-" size (grain domain, etc.) and the "macro-" system size is low, and strong fluctuations are expected from piece to piece.

In that context, the present modeling of amorphous plasticity as a depinning phenomenon is of high interest. As any phase transition, the depinning transition exhibit finite-size

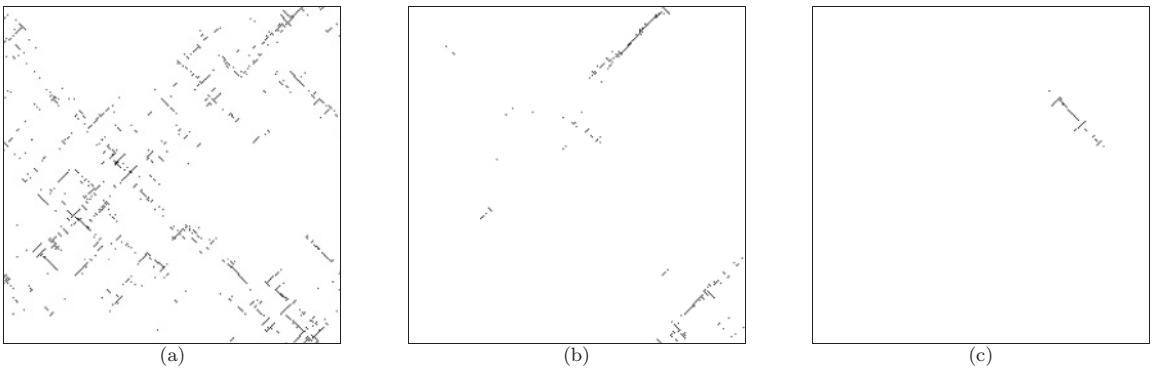

FIG. 4. Maps of cumulated plastic activity during avalanches obtained with stiffness values (from left to right) $K = 10^{-1}$, 10^0, and 10^1 for a system of size $L = 256$. The avalanche sizes were measured to be $S = 1616$, 324, and 81, respectively.

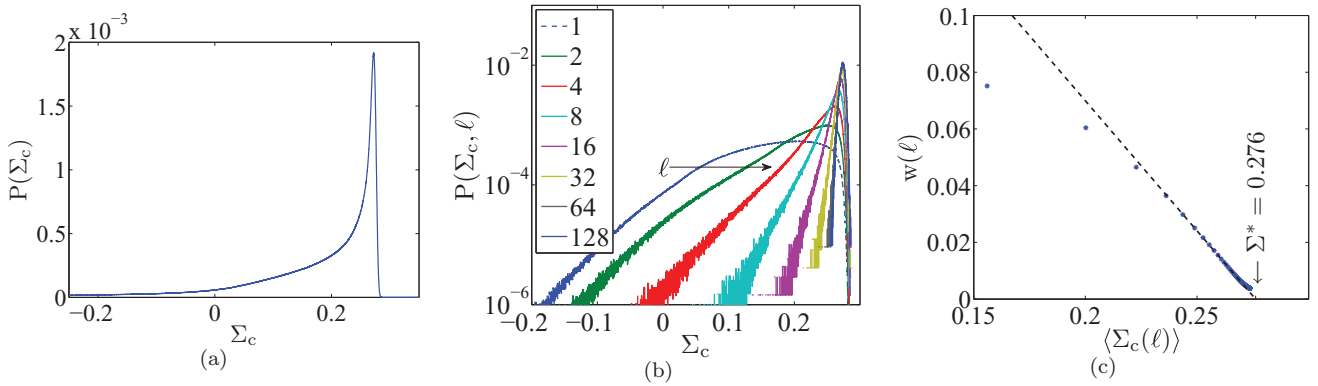

FIG. 5. (Color online) (a) Distribution $P(\Sigma_c)$ of the current yield stress Σ_c sampled over time. The macroscopic yield stress Σ^* is given by the maximum of the distribution. (b) Representation in semilogarithmic coordinates of the conditional distributions $P(\Sigma_c,\ell)$ such that the next slip event is located at a distance ℓ from the current point. $P(\Sigma_c,\ell)$ can be interpreted as the distribution of yield stress fluctuations for a subsystem of size ℓ. (c) Dependence of the width w of the distributions $P(\Sigma_c,\ell)$ vs its mean value $\langle\Sigma_c(\ell)\rangle$ for different ℓ. The linear behavior obtained for large values of ℓ allows to estimate the asymptotic yield limit Σ^* through extrapolation to $w = 0$.

effects that can be quantitatively characterized with the help of critical exponents.

In contrast to usual studies of criticality, the present context invites us to focus on the critical threshold rather than on the critical exponents. While the former is reputed of low interest since it depends on the microscopic details, it gives us here the yield stress value at macroscopic scale. The fluctuations of this threshold for finite systems will thus directly give the expected fluctuations of the yield stress for small pieces.

We develop below a study of finite-size effects that follow the lines of previous works about the depinning of elastic lines [42].

As defined in the description of the model, each elementary zone is characterized by a local plastic criterion $\sigma_c(\boldsymbol{x}) = \sigma_\gamma(\boldsymbol{x}) - \sigma_{\rm res}(\boldsymbol{x})$ (where $\boldsymbol{x}$ refers to the spatial location) that can be separated in two contributions: σ_γ corresponds to the yield threshold of the local structure in absence of internal stress; $\sigma_{\rm res}$ is the internal stress induced by the successive plastic reorganizations that have occurred in the material. For each configuration of the system, a loading that does not trigger any local slip event obeys $\Sigma^{\rm ext} < \Sigma_c = \min_{\boldsymbol{x}} \sigma_c(\boldsymbol{x})$ and the macroscopic yield stress is then defined as the maximum value of this macroscopic load over the whole set of configurations, $\Sigma^* = \max \Sigma_c$; when the external stress lies below that value, Σ^*, plastic deformation will eventually stop after a finite strain, while above it the material can flow indefinitely. To recast this definition in the previous language of avalanches, the macroscopic yield stress is the one that corresponds to the existence of an infinite-size avalanche at vanishing stiffness $k = 0$.

The distribution of these current yield stress values $P(\Sigma_c)$ is shown in Fig. 5(a). Note that Σ_c can take here negative or positive values since it is associated with a fluctuating part of the material properties. (Changing the material yield limit will trivially translate both the distribution and the critical threshold Σ^*.) The same distribution is shown in Fig. 5(b) in logarithmic scale. The entire distribution depends on the local yield stress distribution, here a uniform distribution, and hence has no specific value. However, close to its maximum, the distribution contains only information relative to macroscopically pinned or quasipinned configurations. Hence the behavior of the distribution close to the maximum stress contains generic features that are difficult to extract from such a graph.

To isolate those universal features, it is proposed to part the distribution into conditional probability distribution functions depending on a characteristic that signals that the configuration is close to pinning. We chose the distance ℓ between successive slip events as a clear indication of such a pinned configuration. $P(\Sigma_c,\ell)$ is introduced as the fraction of the initial distribution $P(\Sigma_c)$ such that the plastic event occurred at a distance ℓ from the previous one. This trick gives us a simple way of analyzing finite-size effects. Indeed, writing that plastic activity has to move by a distance ℓ simply means that over a domain of extension ℓ, the system has reached a pinned configuration. $P(\Sigma_c,\ell)$ thus gives direct access to the distribution of effective thresholds for systems of size ℓ. We observe that the larger the distance (the system size), ℓ, the narrower the distribution $P(\Sigma_c,\ell)$ and the closer its center from the maximum of the distribution $P(\Sigma_c)$. This observation is rationalized in Fig. 5(c), where the width of these conditional distributions is plotted against their mean. We obtain a linear behavior, i.e., these two quantities obey the same scaling. In particular, this means that extrapolating this linear behavior to a zero width (which would be obtained for an infinite system) allows us to give a precise estimate of the critical threshold Σ^*.

The precise knowledge of the critical threshold gives us the opportunity to characterize not only the scaling behavior of the finite-size fluctuations of the yield stress but also of the distance between the mean yield stress and the critical threshold. The two scaling behaviors are displayed in Fig. 6. We see that for a typical size ℓ both the width $w(\ell)$ of the yield stress fluctuations and the distance to threshold $\Sigma^* - \Sigma_c(\ell)$ obey the same scaling:

$$w(\ell) \propto \ell^{-b}; \quad \Sigma^* - \Sigma_c(\ell) \propto \ell^{-b} \quad \text{with} \quad b \approx 0.94. \qquad (7)$$

The macroscopic yield stress is hampered by finite-size systematic corrections roughly inversely proportional to the system size. While in the context of elastic line depinning, a similar power-law correction was observed, the exponent b

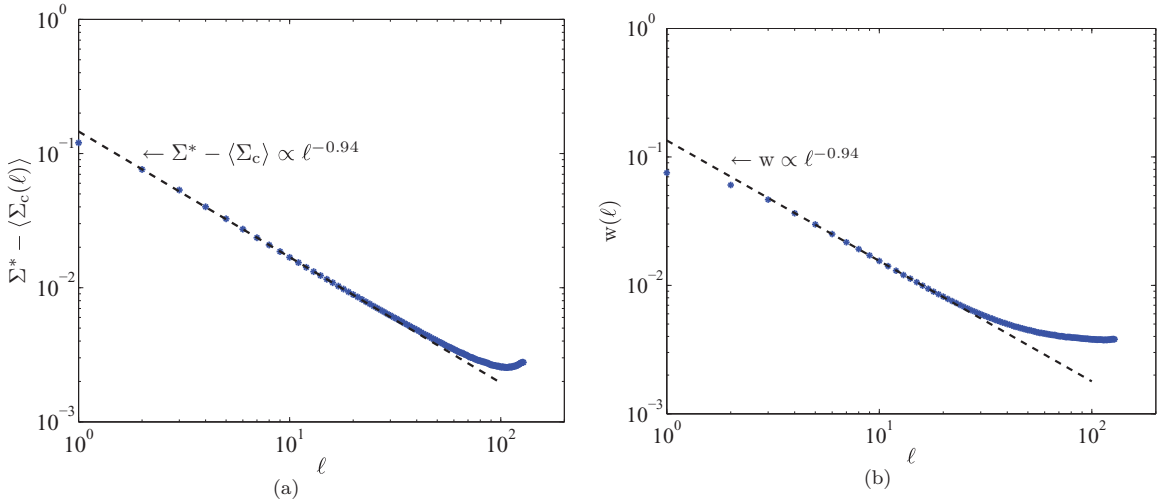

FIG. 6. (Color online) (a) The difference between the asymptotic macroscopic yield stress Σ^* and the mean yield stress $\langle\Sigma_c(\ell)\rangle$ vs distance ℓ, for a system of size $L = 256$. A power-law fit of exponent $b \approx 0.94$ is shown as a dotted line. (b) Plot of the standard deviation of depinning stress w as a function of the distance ℓ, for a system of size $L = 256$. A similar power-law fit of exponent $b \approx 0.94$ is shown as a dotted line.

could be related to the roughness exponent [42], but in the present case, we could not build a similar scaling relation.

V. PLASTIC PRECURSORS

As discussed in Ref. [16], the plastic strain obeys a strong anisotropic scaling resulting from the quadrupolar symmetry of the elastic stress redistribution. Most of the plastic events occur consecutively to a previous plastic event located along a direction at $\pm\pi/4$ (maximum shear directions).

However, it appears that only a tiny fraction of the sites are prone to slip. It is possible to distinguish these precursory sites when looking at the full distribution of the local plastic thresholds $\sigma_c(\boldsymbol{x})$. Such distributions are displayed in Fig. 7(a) for different system sizes. The dashed vertical line at the abscissa of the critical threshold σ^* allows us to separate two populations. The left part corresponds to the weakest sites of the lattice. For one particular configuration, the weakest site gives the current yield stress Σ_c. The right part corresponds to the subcritical sites, their local threshold being larger than the critical value Σ^* they are unconditionally stable. For one configuration, however, not only the weakest site but also a few others can be characterized by a overcritical local threshold, i.e., $\sigma_c(\boldsymbol{x}) < \Sigma^*$. They are thus very likely to initiate a slip event and hence can be termed "precursors." A scaling analysis of this population is of interest. It is clear from Fig. 7(a) that the fraction of precursors decreases when the size L of the system increases. The Fig. 7(b) shows the size dependence of this population in logarithmic scale. We obtain $P[\sigma_c(\boldsymbol{x}) < \Sigma^*] \propto L^{-s}$ with $s \approx 1.34$. This scaling can

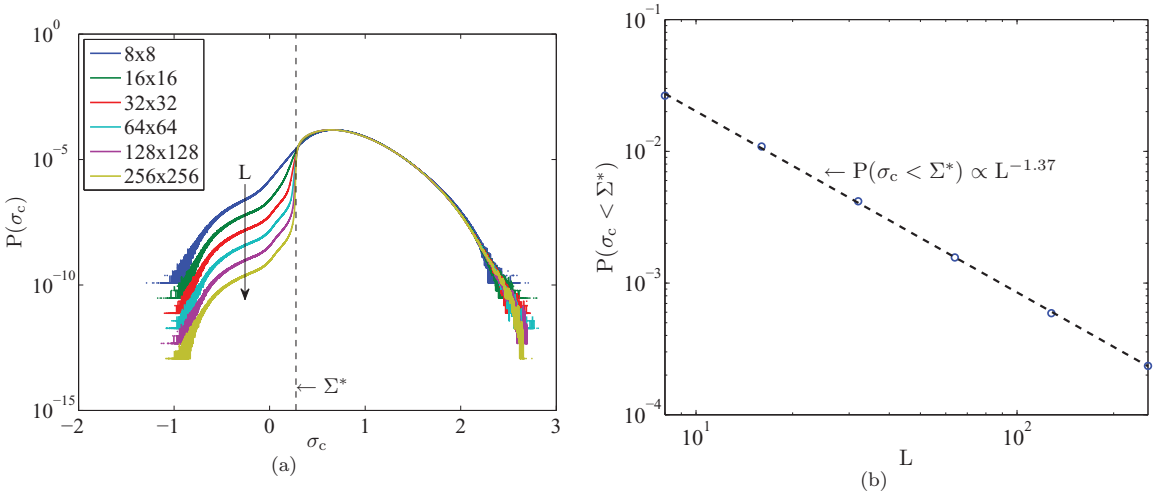

FIG. 7. (Color online) (a) Distribution of individual depinning stress $P(\sigma_c(\boldsymbol{x}))$ for different system sizes $L = 8$, 16, 32, 64, 128, and 256. The dotted line indicates the macroscopic yield threshold Σ^*: The overcritical part ($\sigma_c < \Sigma^*$) depends on L (in contrast to the subcritical one). (b) The relative weight of the overcritical part $P(\sigma_c < \Sigma^*)$ is observed to scale as a power law of the system size. $P(\sigma_c < \Sigma^*) \propto L^{-s}$ with $s \approx 1.34$.

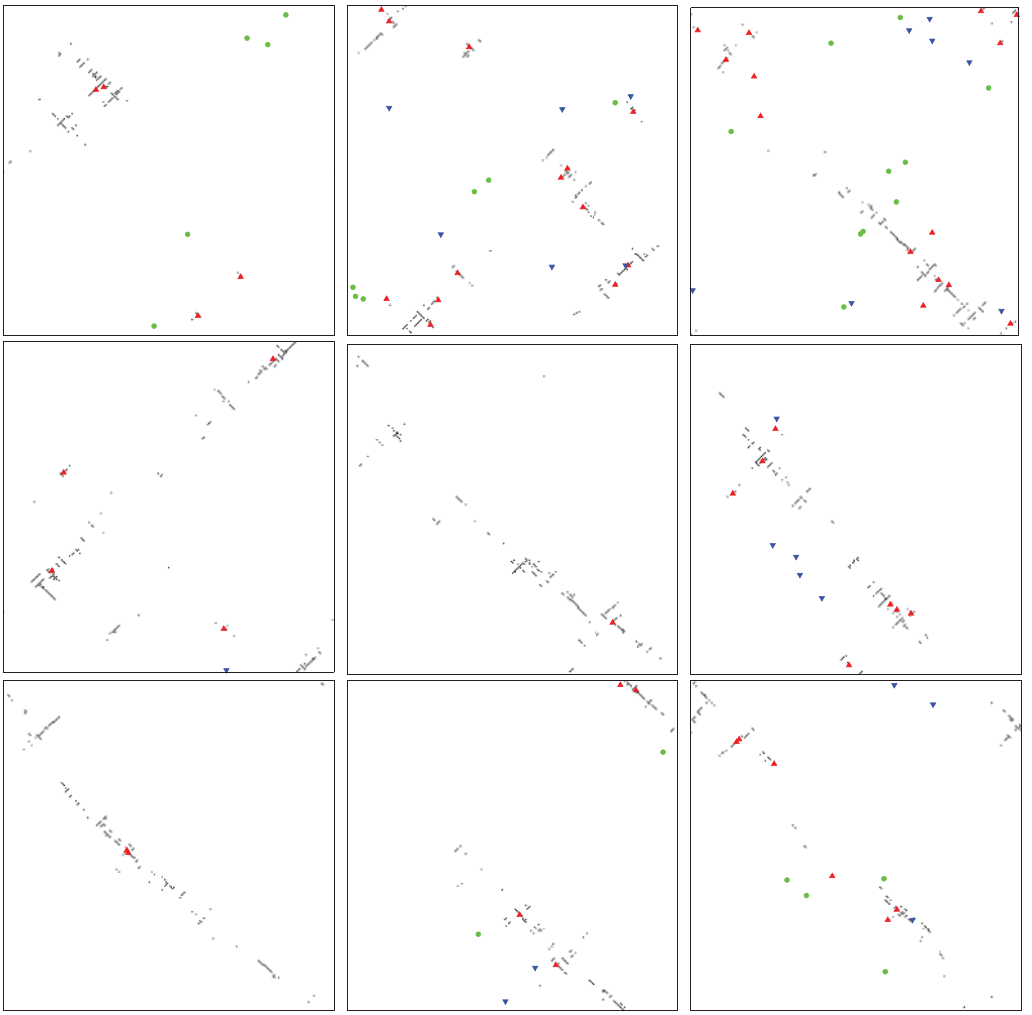

FIG. 8. (Color online) Maps of cumulated plastic activity during avalanches obtained with stiffness values $K = 1$ for a system of size $L = 256$. The colored symbols indicate the location of precursors just before the avalanche takes place. Red upward triangles are part of the avalanche; green and blue symbols are not part of the avalanche, but at the end of the latter green dots are still overcritical while blue downward triangles are no longer over-critical, they have been healed during the avalanche.

be interpreted as the fact that these precursory sites live on a fractal support of dimension $d_F = 2 - s \approx 0.66$.

The identification of a set of precursors can be illustrated graphically. In Fig. 8 we superimposed the plastic activity observed during avalanches with the set of identified precursors (represented as colored symbols) just before the avalanche take place. One can clearly see that avalanches indeed initiate from some of these overcritical sites. One also observes a striking intermittence of this population, which can fluctuate from one to a few tens. It is of interest to follow the fate of these precursors during the avalanche. The red upward triangle indicate sites taking part in the avalanche. Blue and green symbols indicate sites not taking part of the avalanche, but at the end of the latter, green dots are still overcritical while blue downward triangles are no longer overcritical. This possibility of healing is a specificity of the present model. Indeed, in contrast to the case of a depinning front where elastic coupling does not change sign, the quadrupolar interaction is positive or negative depending on the direction and thus has either a stabilizing effect (overcritical sites are sent back in the subcritical part of the distribution) or a destabilizing effect. However, the presence of greens dots indicate that not all overcritical sites are exhausted during an avalanche. Only late plastic events will be initiated there. A large part of the dynamics of the model is thus related to this population of precursors, which seems to encode a long-term information.

VI. CONCLUSION

The present mesomodel of amorphous plasticity, based on the competition between a local yield stress randomness and long-range elastic interaction allowed us to obtain nontrivial results about avalanche statistics and finite-size effects. In particular, the exponent reported here for the scale-free avalanche distribution, $\kappa \approx 1.25$ is significantly different from the mean-field value $(3/2)$. This suggests that a faithful account of the elastic stress redistribution due to local restructuring is indeed a crucial ingredient in the modeling of amorphous plasticity to capture faithfully collective effects. Although original due to this quadrupolar interaction, the present model can still be discussed in the framework of the depinning transition. This allowed us to track the finite-size fluctuation

and systematic size effect of the macroscopic yield stress. In addition, a set of precursory sites of having a fractal support has been identified.

ACKNOWLEDGMENT

V.P. and M.T. acknowledge the support of ANR grant NT-05-0367.

[1] M. Miguel, A. Vespignani, S. Zapperi, J. Weiss, and J.-R. Grasso, Nature (London) **410**, 667 (2001).
[2] M. Zaiser, Adv. Phys. **55**, 185 (2006).
[3] D. Bonamy, J. Phys. D: Appl. Phys. **42**, 2114014 (2009).
[4] J. Schmittbuhl, S. Roux, J. P. Vilotte, and K. J. Måløy, Phys. Rev. Lett. **74**, 1787 (1995).
[5] P. Daguier, E. Bouchaud, and G. Lapasset, Europhys. Lett. **31**, 367 (1995).
[6] S. Ramanathan, D. Ertaş, and D. S. Fisher, Phys. Rev. Lett. **79**, 873 (1997).
[7] D. S. Fisher, Phys. Rep. **301**, 113 (1998).
[8] M. Zaiser, Mater. Sci. Eng. A **309–310**, 304 (2001).
[9] J.-C. Baret, D. Vandembroucq, and S. Roux, Phys. Rev. Lett. **89**, 195506 (2002).
[10] P. Moretti, M. C. Miguel, M. Zaiser, and S. Zapperi, Phys. Rev. B **69**, 214103 (2004).
[11] A. S. Argon, Acta Metall. **27**, 47 (1979).
[12] M. L. Falk and J. S. Langer, Phys. Rev. E **57**, 7192 (1998).
[13] C. E. Maloney and A. Lemaître, Phys. Rev. Lett. **93**, 016001 (2004).
[14] A. Tanguy, F. Leonforte, and J.-L. Barrat, Eur. Phys. J. E **20**, 355 (2006).
[15] D. Rodney and C. A. Schuh, Phys. Rev. Lett. **102**, 235503 (2009).
[16] M. Talamali, V. Petäjä, S. Roux, and D. Vandembroucq, e-print arXiv:1005.2463 (2010).
[17] G. Picard, A. Ajdari, F. Lequeux, and L. Bocquet, Phys. Rev. E **71**, 010501(R) (2005).
[18] M. Talamali, V. Petäjä, D. Vandembroucq, and S. Roux, Phys. Rev. E **78**, 016109 (2008).
[19] J. D. Eshelby, Proc. Roy. Soc. A **241**, 376 (1957).
[20] C. E. Maloney and M. O. Robbins, J. Phys. Condens. Matter **20**, 244128 (2008).
[21] C. E. Maloney and M. O. Robbins, Phys. Rev. Lett. **102**, 225502 (2009).
[22] P. Bak, *How Nature Works* (Copernicus Press, New York, 1996).
[23] J. P. Sethna, K. Dahmen, S. Kharta, J. A. Krumhansl, B. W. Roberts, and J. D. Shore, Phys. Rev. Lett. **70**, 3347 (1993).
[24] S. Zapperi, P. Cizeau, G. Durin, and H. E. Stanley, Phys. Rev. B **58**, 6353 (1998).
[25] T. Richeton and J. Weiss, Acta Mater. **53**, 4463 (2006).
[26] T. Richeton, P. Dobron, F. Chmelik, J. Weiss, and F. Louchet, Mater. Sci. Eng. A **424**, 190 (2006).
[27] D. Dimiduk, C. Woodward, and R. L. M. Uchic, Science **26**, 1188 (2006).
[28] B. A. Sun, H. B. Yu, W. Jiao, H. Y. Bai, D. Q. Zhao, and W. H. Wang, Phys. Rev. Lett. **105**, 035501 (2010).
[29] M. Zaiser and P. Moretti, J. Stat. Mech.: Theory Exp. (2005) P08004.
[30] M. Zaiser and N. Nikitas, J. Stat. Mech.: Theory Exp. (2007) P04013.
[31] O. U. Salman and L. Truskinovsky, Phys. Rev. Lett. **106**, 175503 (2011).
[32] A. Lemaître and C. Caroli, Phys. Rev. Lett. **103**, 065501 (2009).
[33] J. Chattoraj, C. Caroli, and A. Lemaître, Phys. Rev. Lett. **105**, 266001 (2010).
[34] E. R. Homer, D. Rodney, and C. A. Schuh, Phys. Rev. B **81**, 064204 (2010).
[35] K. A. Dahmen, Y. Ben-Zion, and J. T. Uhl, Phys. Rev. Lett. **102**, 175501 (2009).
[36] Y. Ben-Zion and J. R. Rice, J. Geophys. Res. **98**, 14109 (1993).
[37] M. Paczuski, S. Maslov, and P. Bak, Phys. Rev. E **53**, 414 (1996).
[38] A. Tanguy, M. Gounelle, and S. Roux, Phys. Rev. E **58**, 1577 (1998).
[39] D. Bonamy, S. Santucci, and L. Ponson, Phys. Rev. Lett. **101**, 045501 (2008).
[40] L. Laurson, S. Santucci, and S. Zapperi, Phys. Rev. E **81**, 046116 (2010).
[41] A. Lemaître and C. Caroli, e-print arXiv:cond-mat/0609689v1 (2006).
[42] D. Vandembroucq, R. Skoe, and S. Roux, Phys. Rev. E **70**, 051101 (2004).